aerospace

IMPACT FACTOR 2.2

CITESCORE 4.0

Article

Accelerated Refueling of Type IV Hydrogen Pressure Tanks by Passive Means: Thermal Material Characterization and Evaluation

Nico Liebers and Sven Ropte

Special Issue

15th EASN International Conference on Innovation in Aviation & Space Towards Sustainability Today and Tomorrow

Edited by

Prof. Dr. Spiros Pantelakis, Prof. Dr. Andreas Strohmayer and Prof. Dr. Gustavo Alonso-Rodrigo

MDPI

https://doi.org/10.3390/aerospace13050403

aerospace

MDPI

Article

Accelerated Refueling of Type IV Hydrogen Pressure Tanks by Passive Means: Thermal Material Characterization and Evaluation †

Nico Liebers * and Sven Ropte

German Aerospace Center (DLR), Institute of Lightweight Structures, Lilienthalplatz 7, 38108 Braunschweig, Germany

* Correspondence: nico.liebers@dlr.de

† This paper is an extended version of our paper published in "Liebers, N.; Ropte, S. Accelerated refueling of type IV hydrogen pressure tanks by passive means: Thermal material characterization and evaluation. In Proceedings of the 15th EASN International Conference, in Madrid, Spain, 14–17 October 2025".

Abstract

The significant heat generated during the refueling of hydrogen pressure tanks may exceed the permissible 85 °C temperature limit for type IV tanks. Common countermeasures such as hydrogen pre-cooling or long filling times are energy- and time-consuming; hence, in this paper, passive means through thermally better-suited materials are examined. State-of-the-art and alternative materials are first characterized and finally compared using a transient heat model. Different material combinations are compared in terms of the maximum temperature and weight in a typical filling scenario. As alternative liner materials, thermoplastics filled with short carbon fibers, minerals, and graphite were selected to improve thermal properties. For the composite overwrap, copper-coated carbon fibers were chosen. The findings show that the liner is the bottleneck while transferring heat from the inner to the outer tank surface. Using graphite-filled thermoplastics as the liner material shows the greatest potential regarding thermal optimization with only a slight weight increase. Using copper-coated carbon fibers additionally further reduces the maximum temperature but results in a significant weight increase.

Keywords: composite manufacturing; hydrogen pressure vessel; thermal management; thermal conductivity

Academic Editors: Spiros Pantelakis, Andreas Strohmayer and Gustavo Alonso-Rodrigo

Received: 27 February 2026
Revised: 7 April 2026
Accepted: 15 April 2026
Published: 24 April 2026

1. Introduction

Hydrogen is one of the emerging renewable energy carrier options, as its refueling consumes less time than recharging batteries. For mobile applications, pressurized hydrogen tanks are widely used due to their technical maturity, robustness and cost advantages [1–4].

Hydrogen pressure tanks can be classified into types I to V, as shown in Figure 1. Type I corresponds to an all-metal tank and Type II to a metallic tank with a carbon fiber-reinforced plastic (CFRP) overwrap in the cylindrical area. Types III and IV consist of a complete composite overwrap with a metallic and thermoplastic liner, respectively. Type V tanks are composite-only tanks, but they are not yet technologically mature and remain the focus of development [3,5].

The gravimetrical storage capacity and storage pressure increase from type I to type IV; hence, type IV is the most widely used type of pressure storage in mobile applications [5].

The thermoplastic liner—commonly PA or HDPE—is used as a mandrel during manufacturing by fiber winding and then acts as a hydrogen permeation barrier and contributes only marginally to mechanical strength [5]. While the thermoplastic liner of type IV tanks provides a better fatigue resistance, hydrogen permeability is higher and thermal conductivity—the focus of this paper—is lower that of the metallic liners of type III tanks.

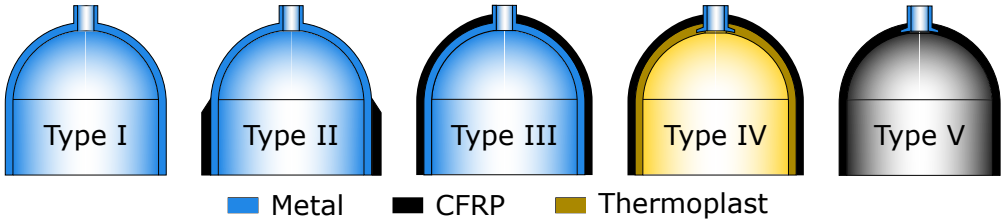

Figure 1. Pressure tank types I to V.

During the refueling of hydrogen into pressure tanks, a significant amount of heat is released due to the high flow friction, the Joule–Thomson effect and compression work [6,7], which is then transferred into the tank structure. Standards exist for automobile applications [8,9], where the temperature rise must not exceed 85 °C. Hence, fast refueling often requires mitigation measures, such as hydrogen pre-cooling, multi-stage fills with lower initial fill rates to reduce flow velocities and active cooling of the tank structure. These measures lead to higher energy consumption and cost and might increase filling duration. Additionally, filling proceeds only until the storage pressure is reached, after which the gas cools, leading to a pressure drop, so the intended state of charge (SOC) is not reached [7,10–13].

Therefore, this paper focuses on improving the thermal properties of the tank structure, particularly its thermal conductivity and heat capacity. There are numerous publications on the thermal aspects of refueling Type III and IV tanks; many focus on complex CFD real-gas simulations, often using material properties from the literature. Heat development and distribution depend strongly on the tank, nozzle and general fueling geometry, as well as on fill rate and other parameters [7,10–16].

A promising approach is to use filled thermoplastics as liner material, as examined in Rosen's PhD thesis [3] in the context of Type IV tanks for automotive applications. Not only the thermal conductivity but also the hydrogen permeability can be improved by fillers. The enhancement of the thermal conductivity of thermoplastics by adding fillers is the focus of numerous publications [17–23]. Other studies analyzed the use of phase-change material to reduce the temperature peak during refueling, but they are limited to theoretical analysis using simulation [24–26], while experimental studies in the context of refueling hydrogen pressure tanks are not known. Blanco-Aguilera et al. [10] analyzed the sensitivity of thermoplastic liner material properties by varying the volumetric heat capacity and thermal conductivity. They used a reference material and virtually increased both parameters in their simulation. They found that increasing both can eliminate the need for hydrogen pre-cooling.

To improve heat transfer through the composite overwrap, copper-coated carbon fibers show great potential. Also, nickel-coated carbon fibers or modification of the thermoset matrix are possible measures to improve thermal conductivity, but the copper coating shows the strongest effect [27,28].

This article is a revised and expanded version of another paper, which was presented at the 15th EASN International Conference, in Madrid, Spain, in October [29].

2. Materials and Methods

In order to analyze and improve heat transfer through the tank structure, the commonly used and potentially better suited materials are characterized in terms of density, filler content, fiber volume content, heat capacity, thermal conductivity (out-of-plane) and temperature diffusivity (in- and out-of-plane). The obtained material properties were used to model the transient heat transfer through the tank structure during refueling and to compare different material combinations, and thereby to identify materials better suited in terms of thermal performance.

In Table 1, the evaluated materials are listed, starting with different polyamides (PAs) and HDPE, which are commonly used liner materials. Different commercially available polyamides filled with short carbon fibers (CFs), mineral fillers and graphite were analyzed as thermally better-suited liner materials. Regarding the composite overwrap, a reference material and a composite material made from copper-coated carbon fibers (ccCFRPs) were examined. The sample names of the filled thermoplastics include the gravimetric filler content derived from density measurements (see Section 3.1.2).

Table 1. List of examined thermoplastic materials.

Sample Name	Manufacturer or Seller	Commercial Name	Description
PA6_1 PA6_2 PA12	Erwin Telle GmbH, Nürnberg, Germany	Polyamid Guss PA 6 G Polyamid extrudiert PA 6 Polyamid PA 12	molded PA6 extruded PA6 PA 12
HDPE	Reichelt Chemietechnik, Heidelberg, Germany	-	HDPE
PA12_8%CF PA12_15%CF PA12_30%CF	n.a. [1]	n.a. [1]	PA12 with 8% carbon fiber PA12 with 15% carbon fiber PA12 with 30% carbon fiber
PA6_Mineral	MOCOM ALCOM, Hamburg, Germany	TCD PA6 5060 FR 16089	PA6 with high mineral filler content
PA66_17%Graphite		PA66 910/32.1 TCE2 BK1282-10	PA66 with graphite filler [2]
PA66_GF_42%Graphite		PA66 910/32.1 GF8 TCE8	PA66 with glass fiber and high graphite filler content [2]
CFRP	Toho Tenax, Wuppertal, Germany	HTS 5631 800tex 12k	Composite reference (with resin below)
ccCFRP	Inca fiber, Chemnitz, Germany	Grafil 34-700 roving (Mitsubishi, Sacramento, CA, USA) with 0.5 µm copper coating [3]	Copper-coated composite (with resin below)
Resin	SICOMIN Composites, Chateauneuf les Martigues, France	SR1710 (resin) and SD8822 (hardener)	Used for CFRP and ccCFRP

[1] Publication of brand name not permitted by manufacturer. [2] Presumably carbon black. [3] Due to time schedule issues, only remaining stock material could be used with uneven coating.

Preparation of Composite Samples

To analyze the composite materials, samples had to be prepared from the fiber material available as rovings. Using a fiber winding process, the rovings were wound unidirectionally onto a steel drum with a diameter of 600 mm (see Figure 2) and manually impregnated with resin using a brush. Both composite material samples, the reference and the copper coated rovings, were prepared at the same time using the same procedure. Afterward, the laminate was removed from the drum, cut into eight squared cutouts and stacked to form a $[0°,\ 90°]_{4s}$ layup. Curing occurred under a vacuum bag using a caul plate, first under room temperature for 24 h and then in an oven at 80 °C for 8 h.

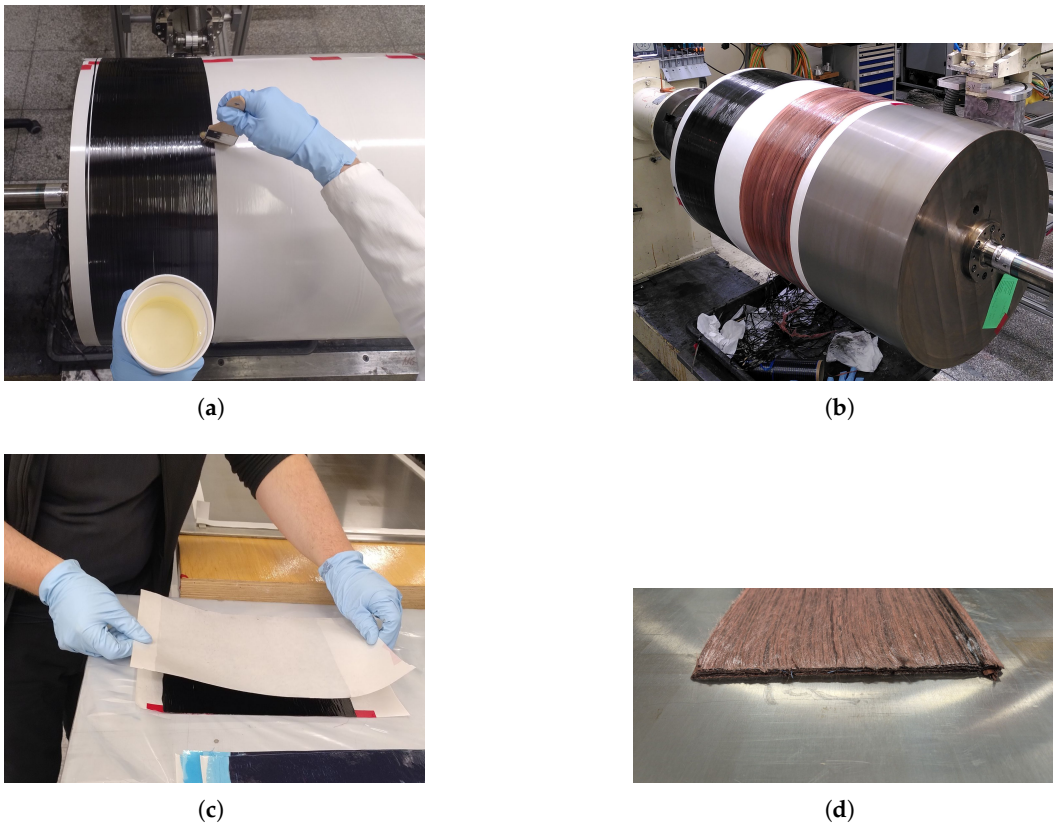

(**a**) (**b**) (**c**) (**d**)

Figure 2. Preparation of composite samples by fiber winding: (**a**) Manual impregnation of fibers using brush. (**b**) Fiber winding of carbon fiber and copper-coated carbon fiber on a drum. (**c**) Layup after cutting. (**d**) Finished layup of copper coated fiber.

3. Results

3.1. Material Characterization

3.1.1. Fiber Volume Content

The two composite samples CFRP and ccCFRP manufactured as described above were analyzed for their fiber volume content by thermogravimetric analysis (TGA) following ISO11385 [30] using a TGA/DSC 3+ (Mettler Toledo, Columbus, OH, USA). The TGA started by drying the samples at 120 $^{\circ}C$ for 120 min under a nitrogen atmosphere, after which the dry mass m_{tot} was measured. The samples were then continuously heated at 10 $K \cdot min^{-1}$ in an oxygen atmosphere to 450 $^{\circ}C$ and held at that temperature for 230 min at that temperature to remove the thermoset matrix and determine the mass of the fibers m_F. The fiber ϱ_F and sample densities ϱ_{tot} were measured using the buoyancy principle (see Section 3.1.2). The fiber volume content is calculated by:

$$\Phi = \frac{V_F}{V_{tot}} = \frac{m_F \cdot \varrho_{tot}}{\varrho_F \cdot m_{tot}} \quad (1)$$

The results are listed in Table 2. For the reference CFRP sample, the achieved FVC of 48.6% is acceptable, but for the ccCFRP sample, the FVC of 27.8% is too low. The low FVC is assumed to be due to excessive resin that could not bleed out because of blocked flow paths, a lack of absorption material and insufficient pressure during curing under vacuum. The ccCFRP sample was used for material characterizations, but for comparing different materials in the thermal simulation, due to the insufficient FVC values reported by Bard [27,28] that were used. Due to the time schedule, the sample preparation could not be repeated.

Table 2. Results of fiber volume measurement.

Sample	ϱ_{tot} $\left[\frac{\text{kg}}{\text{m}^3}\right]$	m_{tot} [mg]	ϱ_F $\left[\frac{\text{kg}}{\text{m}^3}\right]$	m_F [mg]	Φ_F [%]	$\bar{\Phi}_F \pm \sigma$ [%]
CFRP	1432	135.89	1780	81.37	47.9	48.6 ± 0.48
	1438	135.06		83.57	49.0	
	1444	139.38		84.41	48.9	
ccCFRP	1803	432.22	3047	203.58	27.9	27.8 ± 0.14
	1709	428.11		200.53	27.7	
	1778	426.25		204.48	28.0	

3.1.2. Density and Filler Content

The density was measured using the Archimedes principle (buoyancy principle) using an AX205 DeltaRange balance (Mettler Toledo, Columbus, OH, USA). Weights were measured in air m_1 and in distilled water m_1 with known density ϱ_F. The density ϱ can be calculated by:

$$\varrho = \frac{m_1 \varrho_F}{m_1 - m_2} \tag{2}$$

The densities of three samples of each material were determined and the results are plotted in Figure 3. The materials are ordered and grouped and aluminum is shown for comparison as a commonly used Type III tank liner material. PA and HDPE are the commonly used thermoplastic liner materials. As the results show, HDPE has the lowest density, and for PA, the density depends on the type. Because the fillers have a higher density than the thermoplastic matrix (Table 3), density is increased—in some cases significantly, most prominent for the PA6 sample with mineral filler. Regarding the copper-coated carbon fiber composites, they lead to a high density rise depending on fiber volume content up to the level of aluminum.

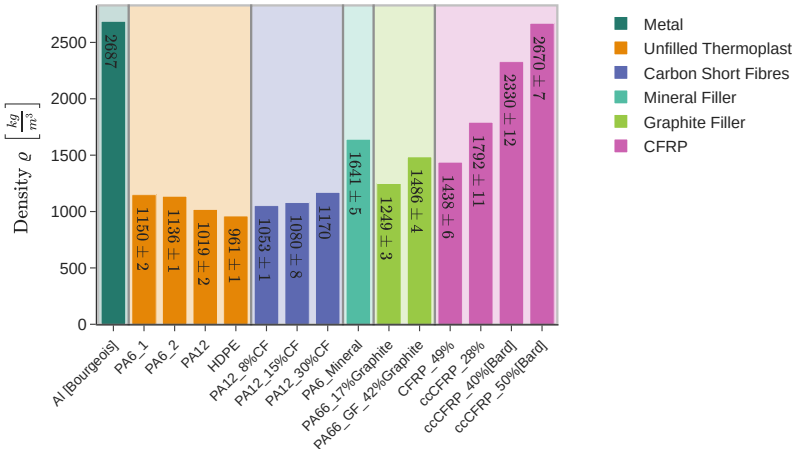

Figure 3. Results of density measurement.

The filler mass content Ψ and filler volume content Φ are defined and can be calculated from the measured densities (index F for filler and M for matrix):

$$\Psi = \frac{m_F}{m_F + m_M} = \frac{\varrho_F(\varrho - \varrho_M)}{\varrho(\varrho_F - \varrho_M)} \tag{3}$$

$$\Phi = \frac{V_F}{V_F + V_M} = \frac{\varrho - \varrho_M}{\varrho_F - \varrho_M} = \frac{\varrho}{\varrho_F}\Psi \tag{4}$$

The results are listed in Table 3. The PA66 sample with high graphite content also contains 8%$_{wt}$ glass fiber ($\varrho_{GF} = 2550$ kg $\cdot$ m^{-3} [31]), so the following relation was taken into account to calculate the graphite filler content:

$$\Psi_{GF} = \frac{m_{GF}}{m_F + m_{GF} + m_M} = \frac{8}{100} \tag{5}$$

$$m_{GF} = \frac{2}{23}(m_F + m_M) \tag{6}$$

Table 3. Calculated filler contents from measured densities.

Sample	$\varrho_F \left[\frac{kg}{m^3}\right]$	$\varrho_M \left[\frac{kg}{m^3}\right]$	$\varrho \left[\frac{kg}{m^3}\right]$	Φ [%]	Ψ [%]
PA12_8%CF	1780	1019	1053	4.7	7.6
PA12_15%CF			1080	8.0	13.2
PA12_30%CF			1170	19.8	30.2
PA66_17%Graphite	2200 [3]	1150	1249	9.4	16.6
PA66_GF_42%Graphite			1486	27.0	41.5

3.1.3. Heat Capacity

Heat capacity was measured using dynamic scanning calorimetry (DSC) and the TOPEM method [32], in which modulated random temperature pulses are added to the constant temperature rate. By analyzing the phase of the response, the heat capacity can be derived. The heat capacity is measured over the range 0 °C $\leq T \leq$ 100 °C in 1 K intervals using a DSC 2 (Mettler Toledo, Columbus, OH, USA).

Figure 4 shows the average volumetric heat capacity of three samples of each material at five chosen temperatures. The volumetric heat capacity c_v is chosen for comparison in Section 3.2; the same geometry and hence volume is used for all materials. Therefore, the volumetric heat capacity is the relevant parameter and is defined by:

$$c_v = c_p \cdot \varrho \left[\frac{J}{m^3 \cdot K}\right] \tag{7}$$

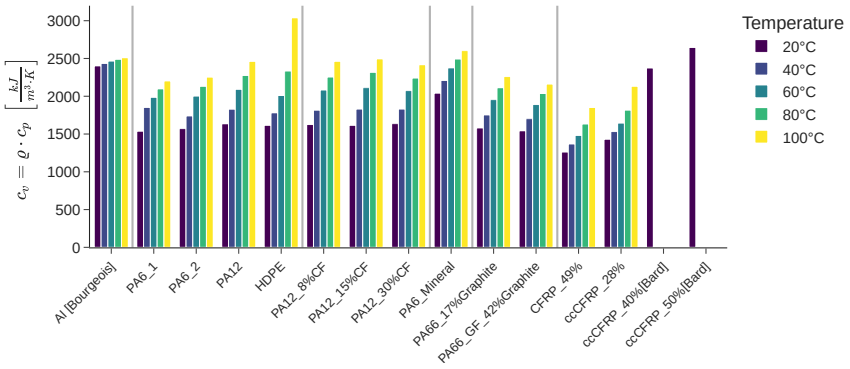

Figure 4. Results of volumetric heat capacity (from specific heat and density measurement) at different temperatures.

All materials show a monotonically increasing heat capacity as temperature rises. The values reported by Bard [27,28] are available only at 20 °C and are presumed to increase with temperature as well. The lack of temperature-dependent data will hence lead to higher temperatures in the thermal model. This effect is most prominent for HDPE, which reaches the highest overall value at 100 °C, making it a good candidate as a liner material for heat absorption. Aluminum shows low temperature dependence and relatively high volumetric heat capacity values.

The carbon fiber-filled PA12 materials have values almost the same as those of unfilled PA12. The mineral-filled PA6 shows lower temperature induced growth at high values and also at low temperatures, while graphite reduces the volumetric heat capacity. The CFRP

samples have a relatively low volumetric heat capacity, which is increased by fiber volume content of copper-coated carbon fibers.

3.1.4. Thermal Conductivity and Temperature Diffusivity

The out-of-plane thermal conductivity $\lambda_{\perp}$ $\left[\mathrm{W \cdot m^{-1} \cdot K^{-1}}\right]$ was measured using the Guarded Heat Flow Method (GHFM) using a GHFM DTC300 (TA Instruments, New Castle, DE, USA) at temperatures $T = \{20, 40, 60, 80\}$ °C. The in-plane and out-of-plane temperature diffusivities $k_{\parallel}$ and $k_{\perp}$ were obtained by the laser flash method (LFA) with an LFA 457 MicroFlash (Netzsch, Selb, Germany) at the same temperatures as for the GHFM. The in-plane results are not used in the thermal model and hence are not included in this paper. The temperature diffusivity and thermal conductivity are related as follows:

$$k = \frac{\lambda}{c_p \cdot \varrho} \left[\frac{\mathrm{m}^2}{\mathrm{s}}\right] \tag{8}$$

The out-of-plane measurement results are plotted in Figure 5. All materials show decreasing values as temperature increases. Comparing the two methods, the values of the respective samples are generally close, with the exception of PA66_GF_42%Graphite. Differences can have numerous causes, such as laser absorption and infrared emissivity for LFA, which might also vary locally due to fillers and fibers. Also, the LFA method assumes no heat loss to the environment, which is avoidable. In the GHFM method, errors can be caused by thermal contact resistance or heat loss at the sample edges. The difference can also be caused by inaccuracies in the heat capacity measurement used to derive the temperature diffusivity from thermal conductivity. PA66_GF_42%Graphite shows the highest value, while copper-coated carbon fiber composites reported by Bard [27,28] also show very high thermal diffusivity, but are only available at 20 °C, which will decrease the thermal model accuracy.

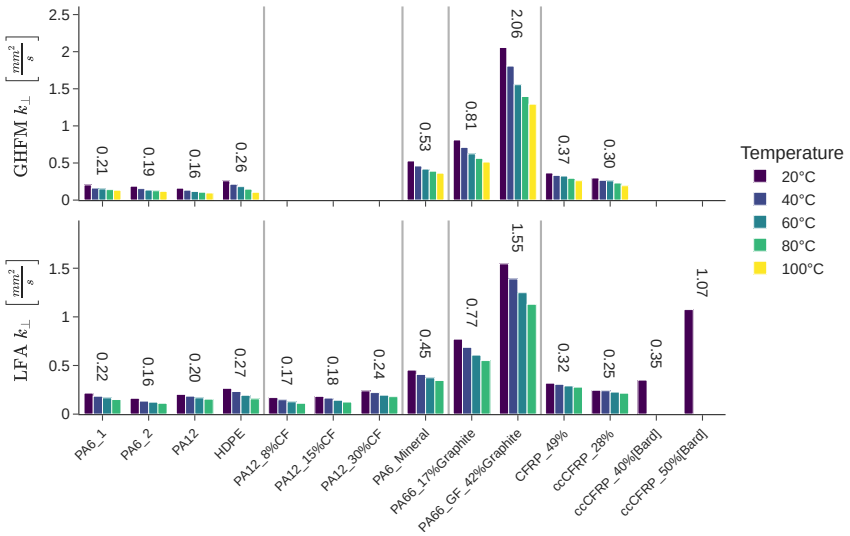

Figure 5. Temperature diffusivity ((**top**): out-of-plane by guarded heat flow method (derived from thermal conductivity), (**bottom**): out-of-plane by laser flash method.

In ref. [33], the temperature diffusivity calculated using Equation (8) is 0.28 $\frac{\mathrm{m}^2}{\mathrm{s}}$ for PA and 0.22 $\frac{\mathrm{m}^2}{\mathrm{s}}$ for HDPE, similar to the obtained values. According to Chen et al. [22] the thermal conductivity of polymers can vary over a wide range (HDPE: $0.33 \leq \lambda \left[\frac{\mathrm{W}}{\mathrm{m \cdot K}}\right] \leq 0.53$, PA6: $0.22 \leq \lambda \left[\frac{\mathrm{W}}{\mathrm{m \cdot K}}\right] \leq 0.33$) depending on the exact molecular architecture and additives. According to the datasheet, the expected in-plane temperature diffusivity for

PA66_GF_42%Graphite is 2.21 $\frac{m^2}{s}$. The value obtained by LFA is much lower and the value measured by GHFM is closer, though still slightly lower.

3.2. Heat Transfer Model

As this study aims to improve fast refueling processes, high hydrogen mass rates are assumed during the refueling process. As Bourgeois et al. [34] summarize in their review paper, at high fill rates and high gas velocities, the temperature distribution can be assumed to be relatively uniform. At these gas velocities, forced convection dominates over natural convection. This assumption is supported by other experimental results [6,13,34–36]. Assuming a homogeneous temperature distribution, 1D radial heat transfer is modeled in the cylindrical part of the tank. This neglects—among other factors—the non-uniform composite-layup over the tank and the influence of the heat transfer through the bosses, which accounts for approximately 23% of the heat transfer [34].

The 1D radial heat transfer equation in cylindrical coordinates is given by [33]:

$$\frac{\partial T}{\partial t} = \frac{1}{r}\frac{\partial}{\partial r}\left(r \cdot k_r \frac{\partial T}{\partial r}\right) + s \tag{9}$$

The explicit finite difference formulation for heterogeneous materials using arithmetic average to calculate the thermal diffusivity between grid points $k_{i+\frac{1}{2}} = \frac{k_i + k_{i+1}}{2}$ is given by [37]:

$$T_i^{n+1} = \frac{1}{2r_i}\frac{\Delta t}{\Delta r^2}\left[(r_i k_i + r_{i+1}k_{i+1})\left(T_{i+1}^n - T_i^n\right) - (r_{i-1}k_{i-1} + r_i k_i)\left(T_i^n - T_{i-1}^n\right)\right] + T_i^n + s_i^n \Delta t \tag{10}$$

where the temperature T_i^{n+1} of the next time step t_{n+1} at grid point r_i depends on the temperatures at the current timestep t_n and the surrounding grid points r_{i-1}, r_i, r_{i+1}, the corresponding temperature diffusivity values k_{i-1}, k_i, k_{i+1} and the source term s_i. The spatial grid is evenly spaced with distance Δr into N grid points with grid point index $0 \leq i \leq N-1$. The time step Δt is constant.

The model scheme is shown in Figure 6. The inner boundary condition was set to a constant heat flux density to model the heat released during refueling. The magnitude $\dot{q} = 4750\ \frac{W}{m^2}$ was estimated by applying the thermal model to the data and the experimental results of Couteau et al. [38] and Monde et al. [39] to match the same inner liner wall end temperature. The details can be found in Appendix A. The temperature at the inner boundary can be calculated by rearranging the energy balance [33]:

$$\dot{q} = -\frac{\lambda_0}{r_0}\frac{T_1 - T_0}{ln\frac{r_1}{r_0}} \tag{11}$$

$$\implies \quad T_0 = T_1 + \frac{\dot{q} r_0 \ln\left(\frac{r_1}{r_0}\right)}{\lambda_0} \tag{12}$$

The outer boundary condition was modelled as convection with a heat transfer coefficient $\alpha = 6\ W \cdot K^{-1} \cdot m^{-2}$ as used in [11] with an ambient temperature of $T_\infty = 20\ °C$. The outer boundary temperature T_{N-1} can hence be calculated by:

$$\alpha(T_{N-1} - T_\infty) = -\frac{\lambda_{N-1}(T_{N-1} - T_{N-2})}{r_{N-1}\ln\left(\frac{r_{N-1}}{r_{N-2}}\right)} \tag{13}$$

$$\implies \quad T_{N-1} = \frac{T_{N-2} \cdot \lambda_{N-1} + T_\infty \cdot \alpha \cdot r_{N-1}\ln\left(\frac{r_{N-1}}{r_{N-2}}\right)}{\alpha \cdot r_{N-1}\ln\left(\frac{r_{N-1}}{r_{N-2}}\right) + \lambda_{N-1}} \tag{14}$$

The initial temperature was set to $T(t=0) = 20\ °C$. The material properties c_p and k or respectively λ are updated in every time step depending on the current temperature

using a polynomial fit on measured values. The simulation time was $t_{max} = 180$ s with a time step Δt depending on the Courant–Friedrichs–Lewy stability criterion Δt_{crit} [37] $\Delta t = 0.8 \cdot \Delta t_{crit}$:

$$\Delta t = 0.8 \cdot \Delta t_{crit} = 0.8 \cdot \frac{\Delta r^2}{2 \cdot k_{max}} \tag{15}$$

The tank geometry of a previous internal project was used, where the dataset of geometry measurements and burst test is published [40]. The cylindrical area of the tank was chosen for the transient heat transfer calculations, with the inner radius of $r_0 = 198$ mm, liner thickness of $t_{liner} = 8$ mm and composite overwrap thickness of $t_{comp} = 26$ mm, using a radial grid spacing of $\Delta r = 0.5$ mm. The heat transfer model was implemented in Python version 3.11.9.

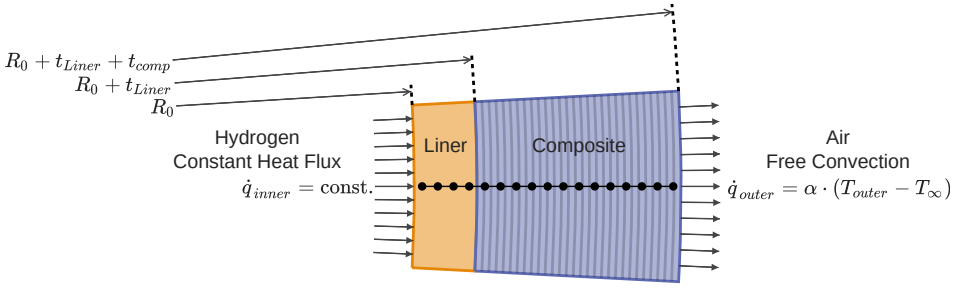

Figure 6. Scheme of the 1D radial finite difference heat transfer model.

Six different material setups were simulated and compared for maximum temperature and weight:

1. Reference–PA6 liner with standard composite;
2. Reference HDPE–HDPE liner with standard composite;
3. Reference Type III–Aluminum liner with standard composite;
4. Mod. Liner–Modified liner with standard composite;
5. Mod. Composite–PA6 liner with modified composite
6. Mod. Liner+mod. Composite–Modified liner and modified composite;
7. Mod. Liner+6 mm mod. Composite–Modified liner with 6 mm modified composite and 20 mm standard composite.

PA6 and HDPE were chosen as reference liner materials, while the material data of PA66_GF_42%Graphite was used for the modified line. For the standard composite the data of CFRP_49% and for the modified composite the data of ccCFRP_50%[Bard] were used.

Figure 7 shows the simulation results of three different tank configurations: (a) the reference configuration with PA6 liner and reference composite overwrap, (b) the configuration with a modified liner and reference composite overwrap and (c) the configuration with a modified liner and modified composite overwrap. For each, the top plot shows temperature profile over the wall thickness after 180 s and the bottom plots show the temperature evolution over time using a color representation. In (d) all scenarios are compared as a temperature plot over the wall thickness after 180 s as well.

The thermal simulation of the reference tank shows a maximum temperature of 107.8 °C at the inner liner surface with a steep temperature gradient inside the liner, with a temperature at the interface between liner and composite of only 34.7 °C, while at the outer surface the heat-up is negligible.

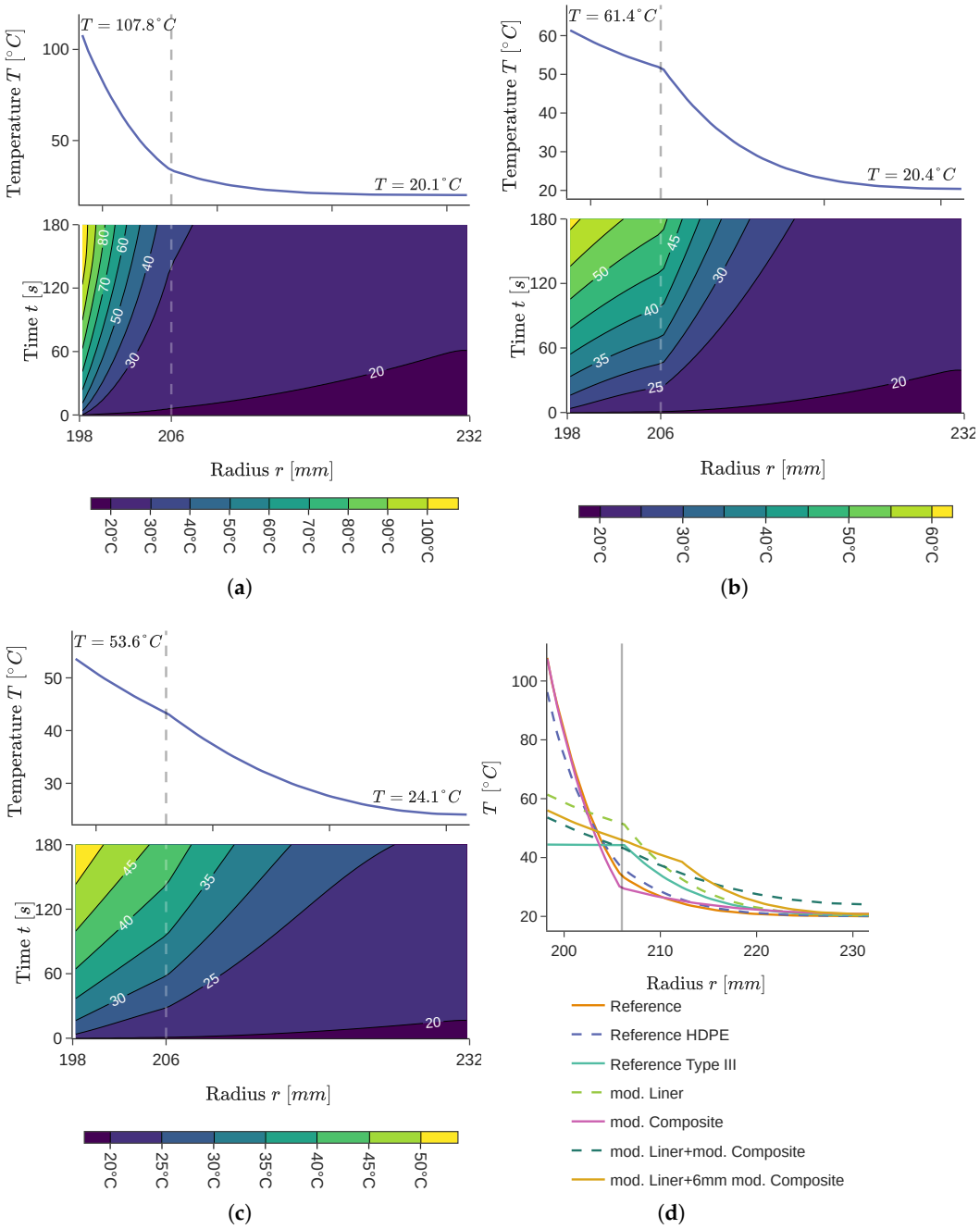

Figure 7. Comparison of simulation results (for (**a**–**c**) top: temperature profile over radius at end of refueling, bottom: contour plot of temperature evolution over radius): (**a**) Reference of PA6 liner and composite overwrap. (**b**) Modified liner (PA66_GF_42%Graphite) and composite overwrap. (**c**) Modified liner PA66_GF_42%Graphite) and modified composite overwrap (ccCFRP_50%[Bard]). (**d**) Temperature profile over radius at end for all material setups. Vertical gray lines show interface of liner and composite overwrap.

Using the modified liner with standard composite overwrap, the peak temperature is reduced to 61.4 °C, and due to the higher temperature diffusivity, a higher interface temperature of 52.0 °C is reached, enabling higher heat transfer through the composite. The results of the modified liner and modified composite show that the maximum temperature of 53.6 °C is significantly lower and the composite structure absorbed more heat. The outer boundary temperature of 24.1 °C is still low; hence, the heat transfer into the surroundings is negligible for very fast filling, as other studies have also shown [11,39].

Because the peak temperatures in the first scenarios exceed 100 °C, the simulation results become inaccurate as temperature diffusivity was only measured up to 80 °C and heat capacity up to 100 °C. Assuming continuous trends, the heat capacity would increase, thereby lowering the resulting peak temperature, while the temperature diffusivity would decrease, leading to higher peak temperatures.

The simulation results are compared in Figure 8, showing the maximum temperature and weight per cylinder length. The results show that, from a thermal perspective, HDPE is a better-suited liner material than PA6, leading to a maximum temperature reduction of 11.6 K by even reducing the weight by 2.8%. The Type III tank with aluminum liner achieves the lowest temperature while weighing 25.0% more (assuming the same thickness as for Type IV).

Using the modified liner material PA66_GF_42%Graphite with the standard composite overwrap, the temperature peak is lowered significantly by 46.5 K, leading to 5.6% weight increase. Modifying only the composite results in almost no thermal improvement, but a 70% weight increase. During the short refueling time, the bottle-neck is the thermoplastic liner and hence the heat is not transferred into the overwrap. Using modified material for both the liner and the overwrap can reduce temperature further than only modifying the liner, but it comes at a high weight increase. Finally, using only a modified composite material for the first 6 mm of the overwrap lowers the temperature further than modifying only the liner.

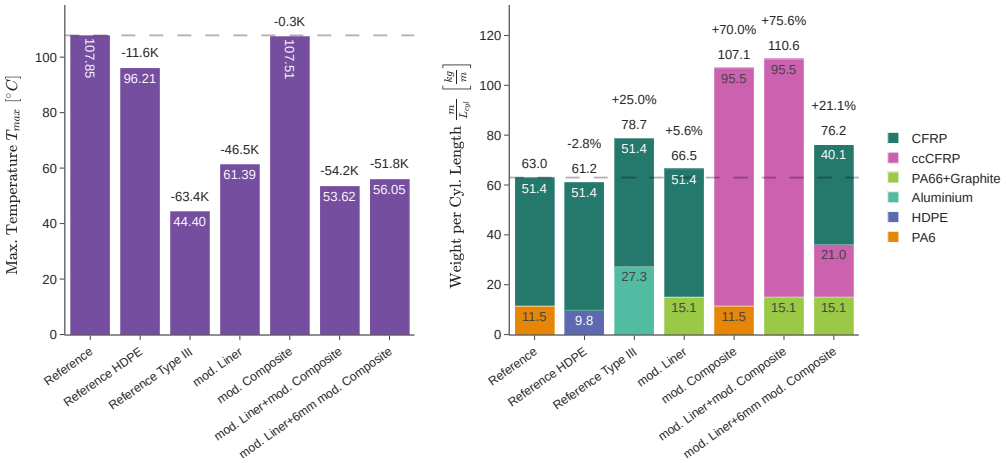

Figure 8. Summary of simulation results of different material combinations with vertical dashed line marking the reference value ((**left**): Maximum temperature after 180 s refueling, (**right**): Weight per cylinder length).

4. Discussion

A simplified approach using only a 1D thermal model was used to compare different material combinations to estimate the potential for improving the transfer of heat released during hydrogen refueling and to decrease the peak temperature. A literature review of CFD simulations and experiments on the heat generation and temperature evolution of hydrogen refueling [7,10–12,14–16] showed that, in many cases, due to the high fluid velocity and turbulent flow, the heat is nearly evenly distributed. This means that a 1D radial heat model provides a good initial estimation for material pre-screening of materials with the potential to accelerate the hydrogen refueling process, while neglecting the effects of local variations in composite stacking and thickness, as well as the influence of the metallic nozzle. Future studies are planned to take those effects into account using a 3D heat model.

As described in Section 3.1.1, due to the low fiber volume content of the composite sample with copper-coated carbon fibers, material properties from the literature had to be used for the thermal model. This introduces uncertainty regarding the comparability of the cited and measured properties, as the measurement methods differ. Also, the cited values are available only at 20 °C, whereas the heat capacity increases and the temperature diffusivity decreases with increasing temperature for all characterized materials. Thus, the quantitative accuracy of the model is limited. However, it is not expected to significantly affect the overall conclusion that modifying the liner material offers the greatest potential for reducing the peak temperature while causing only a small weight increase and requiring only minor modification of the standard configuration.

Modifying the liner by using PA6 filled with graphite seems to be the best option for improving heat transfer and heat absorption during refueling. The weight increase is marginal, while the effect on heat transfer is very positive. Additionally, it has been shown that graphite reduces hydrogen permeability [3,14], which might also allow a reduction in liner thickness. According to Rosen [3], the hydrogen permeability of PA can be reduced by approximately 70% using a similar graphite filler content, but this reduces tensile and bending strength while increasing both moduli. Using filled polymers is expected to increase material and manufacturing cost and might require adapted manufacturing processes due to modified viscosity and cooling properties. The composite overwrap can remain unchanged, so the impact of the modification on mechanical strength is expected to be low, which may facilitate certification. If only the liner has to be modified, the cost increase is expected to be low compared to the overall tank manufacturing cost. A possible risk of higher costs is the manufacturability of liners using the modified thermoplastic, e.g., by rotary molding, due to the lag of experience with this material. In addition, mechanical aspects such as mechanical strength, fatigue and long-term permeability under cyclic stress must be validated.

The presented passive means for improving heat transfer during hydrogen refueling can help reducing refueling times, reaching higher states of charge and decreasing the need for pre-cooling.

Future studies will concentrate on other tank designs like a hybrid Type IV/V tank where the liner is melted under temperature and partially infused into the wound carbon fibers forming a thermoplastic interface before the remaining dry fibers are impregnated with a thermoset matrix [41,42]. This design is expected to provide better thermal contact and also reduces the heat transfer path length. Future research will also include experimental refueling tests on modified tanks integrated with temperature sensors in order to monitor the temperature gradient.

5. Conclusions

The results show that modifying PA6, a commonly used liner material, with graphite filler can significantly decrease the peak temperature during fast hydrogen refueling, indicating that the liner is the bottleneck. The peak temperature was reduced by 46.5 K, while the weight increased by 5.6%. Modifying the composite overwrap with copper-coated carbon fibers has only a minor effect, while the weight gain is relatively high.

The prepared composite samples for this study achieved only a low fiber volume content, necessitating the use of thermal properties from the literature, limiting the accuracy of the model. Additionally, the study uses only a radial 1D thermal model, neglecting tank inhomogeneities; this approach is intended as an initial comparison of material combinations as a preselection of future research using more detailed models and experiments.

Using these results, a preliminary selection of thermally better-suited materials for the refueling of Type IV tanks can be made and used for further investigations. The materials

should be evaluated for suitability in manufacturing tanks, for example, whether liners can be produced using graphite-filled PA6, due to its different viscosity and faster cool-down during rotary or injection molding. The mechanical properties, especially under cyclic stress, should be investigated, as well as their influence on hydrogen permeability. In addition, the thermal performance of tanks with the modified materials must be validated through refueling experiments.

Author Contributions: Conceptualization, N.L. and S.R.; methodology, N.L. and S.R.; software, N.L.; validation, N.L.; formal analysis, N.L.; investigation, N.L. and S.R.; data curation, N.L. and S.R.; writing—original draft preparation, N.L.; writing—review and editing, N.L. and S.R.; visualization, N.L.; supervision, N.L. and S.R.; project administration, N.L. and S.R. All authors have read and agreed to the published version of the manuscript.

Funding: This research received no external funding.

Data Availability Statement: Data is available upon request.

Acknowledgments: The authors would like to thank Hendrik Lange for carrying out a part of the experiments and measurements and Souher Aldroubi for proof-reading. Furthermore, the authors thank MOCOM for providing samples.

Conflicts of Interest: The authors declare no conflicts of interest.

Abbreviations

The following abbreviations are used in this manuscript:

COPV	Composite Overwrapped Pressure Vessels
CF	Carbon fiber
CFRP	Carbon fiber-Reinforced Plastic
ccCFRP	CFRP with copper-coated Carbon fibers
SOC	State of Charge
FVC	fiber volume content
DSC	Differential scanning calorimetry
TGA	Thermogravimetric analysis
PA	Polyamide
HDPE	High-Density Polyethylen

Appendix A. Heat Flux Estimation

As a source of heat, the simple, pragmatic approach was chosen to use a fixed heat flux density $\dot{q}$. The value was estimated using the same 1D radial heat model from Section 3.2 to match the results of one of the experiments by Couteau et al. [38] and two of the experiments by Monde et al. [39], using the respective geometry and material properties. In these experiments sufficient data were provided to simulate the process, and the inner liner temperature was also given. The used data is summarized in Table A1. The material data was only available as temperature-independent.

The two experiments by Monde et al. 2012 [39] both result in a similar value for heat flux density of $\dot{q} = 4750\ \frac{\mathrm{W}}{\mathrm{m}^2}$ and $\dot{q} = 4500\ \frac{\mathrm{W}}{\mathrm{m}^2}$, while for the experiment by Couteau et al. 2022 [38] the estimated heat flux density is only $\dot{q} = 2750\ \frac{\mathrm{W}}{\mathrm{m}^2}$. All three obtained results using the thermal model with a fixed heat flux density show a good match with the results shown in the cited publications by qualitative comparison. The simulation results of reproducing "Test Run #5" by Monde et al. 2012 [39] are shown in Figure A1.

Even though the tank geometries and filling profile is similar, the end temperatures and estimated heat flux differ significantly. These differences could be caused by the experimental set-up, like nozzle diameter, leading to different heat development by friction,

heat loss through different boss design, differences in temperature measurement and difference in pre-cooling the hydrogen gas.

As the presented work aims at accelerating the refueling process, the highest value for heat flux density was chosen to evaluate the characterized materials.

Table A1. Used data for heat flux density estimation.

Value		Couteau et al. 2022 [38] "Experiment 1"	Monde et al. 2012 [39] "Test Run #5"	Monde et al. 2012 [39] "Test Run #6"
Tank Type		Type IV; $V = 36$ l	Type IV; $V = 40$ l	Type IV; $V = 39$ l
Internal radius	R_0 [mm]	129.4	140	140
Liner Thickness	t_{Liner} [mm]	6	5	3
Composite Thickness	t_{Comp} [mm]	25	30	22
Initial Pressure	P_{init} [MPa]	10	2.8	4.75
Final Pressure	P_{end} [MPa]	70	70	70
Filling Time	t_{max} [s]	120	188	180
Initial Temperature	T_0 [°C]	12	20.4	2.6
Final Inner Liner Wall Temperature	T_{max} [°C]	54 (Figure 3 in [38])	70 (Figure 6c in [39])	43 (Figure 7c in [39])
Liner Thermal Conductivity	$\lambda \left[\frac{W}{m \cdot K}\right]$	0.36	1.17	1.17
Liner Temperature Diffusivity	$k \left[\frac{m^2}{s}\right]$	$2.02 \cdot 10^{-7}$	$5.77 \cdot 10^{-7}$ *	$5.77 \cdot 10^{-7}$ *
Composite Thermal Conductivity	$\lambda \left[\frac{W}{m \cdot K}\right]$	0.15	0.66	1.14
Composite Temperature Diffusivity	$k \left[\frac{m^2}{s}\right]$	$6.70 \cdot 10^{-7}$	$4.47 \cdot 10^{-7}$ *	$7.71 \cdot 10^{-7}$ *
Estimated heat flux density	$\dot{q} \left[\frac{W}{m^2}\right]$	2750	4750	4500

* Calculated from given thermal conductivity, heat capacity and density (left: temperature evolution of inner liner wall over filling process, right: temperature profile over tank wall at end of filling).

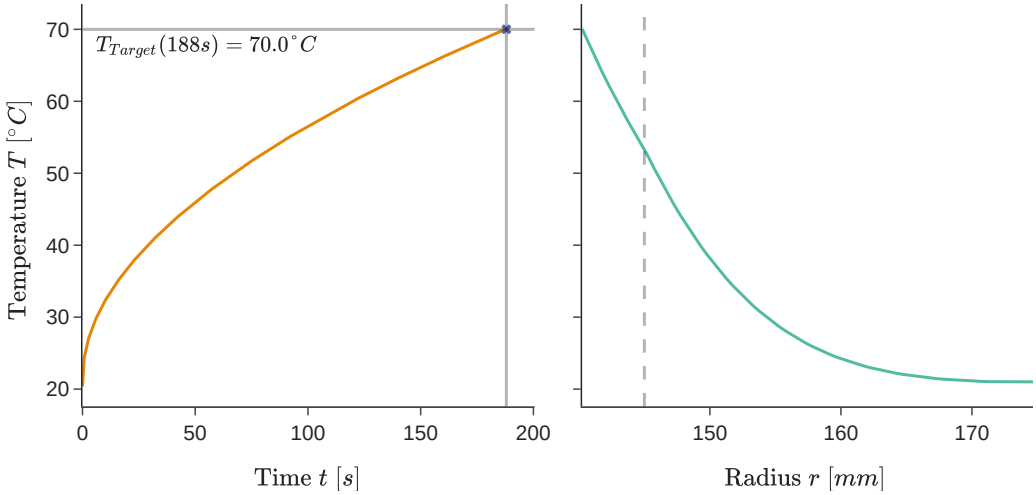

Figure A1. Results of thermal simulation using data from Monde et al. 2012 [39] "Test Run #5" with estimated heat flux of $\dot{q} = 4750 \frac{W}{m^2}$. ((**left**): temperature evolution over time at inner liner wall, vertical and horizontal line mark target time and temperature, (**right**): temperature profile over tank wall at end of simulation, dashed vertical line marks interface of liner and composite overwrap).

References

1. Penavayre, C.; Fitoussi, J.; Richaud, E.; Papin, P.; Bouneb, J.; Hochstetter, G.; Shirinbayan, M. Long–Term Behavior of Carbon Fiber–Reinforced Thermoplastic Composites for Type V Hydrogen Storage Tanks: Effects of Hygrothermal Aging on Physicochemical and Mechanical Properties. *Polym. Compos.* **2025**, *47*, 1484–1497. [CrossRef]

2. Barthelemy, H.; Weber, M.; Barbier, F. Hydrogen storage: Recent improvements and industrial perspectives. *Int. J. Hydrogen Energy* **2017**, *42*, 7254–7262. [CrossRef]
3. Rosen, P.A. Beitrag zur Optimierung von Wasserstoffdruckbehältern. Ph.D. Thesis, Technische Universität Chemnitz, Chemnitz, Germany, 2017.
4. Su, Y.; Lv, H.; Zhou, W.; Zhang, C. Review of the Hydrogen Permeability of the Liner Material of Type IV On-Board Hydrogen Storage Tank. *World Electr. Veh. J.* **2021**, *12*, 130. [CrossRef]
5. Muthukumar, P.; Kumar, A.; Afzal, M.; Bhogilla, S.; Sharma, P.; Parida, A.; Jana, S.; Kumar, E.A.; Pai, R.K.; Jain, I.P. Review on large-scale hydrogen storage systems for better sustainability. *Int. J. Hydrogen Energy* **2023**, *48*, 33223–33259. [CrossRef]
6. Liu, Y.L.; Zhao, Y.Z.; Zhao, L.; Li, X.; Chen, H.g.; Zhang, L.F.; Zhao, H.; Sheng, R.H.; Xie, T.; Hu, D.H. Experimental studies on temperature rise within a hydrogen cylinder during refueling. *Int. J. Hydrogen Energy* **2010**, *35*, 2627–2632. [CrossRef]
7. Li, M.; Bai, Y.; Zhang, C.; Song, Y.; Jiang, S.; Grouset, D.; Zhang, M. Review on the research of hydrogen storage system fast refueling in fuel cell vehicle. *Int. J. Hydrogen Energy* **2019**, *44*, 10677–10693. [CrossRef]
8. UNECE. *Regulation No 134 of the Economic Commission for Europe of the United Nations (UN/ECE)—Uniform Provisions Concerning the Approval of Motor Vehicles and Their Components with Regard to the Safety-Related Performance of Hydrogen-Fuelled Vehicles (HFCV) [2019/795]*; UNECE: Geneva, Switzerland, 2019.
9. Fuel Cell Standards Committee. *Standard for Fuel Systems in Fuel Cell and Other Hydrogen Vehicles*; Fuel Cell Standards Committee: Washington, DC, USA, 2023 [CrossRef]
10. Blanco-Aguilera, R.; Martinez-Agirre, M.; Berasategi, J.; Penalba, M.; Bou-Ali, M.M.; Shevtsova, V. Effect of liner thermal properties and liner pre-cooling on the thermal management of fast-filling of hydrogen tanks. *Int. J. Hydrogen Energy* **2024**, *52*, 1159–1172. [CrossRef]
11. Bourgeois, T.; Brachmann, T.; Barth, F.; Ammouri, F.; Baraldi, D.; Melideo, D.; Acosta-Iborra, B.; Zaepffel, D.; Saury, D.; Lemonnier, D. Optimization of hydrogen vehicle refuelling requirements. *Int. J. Hydrogen Energy* **2017**, *42*, 13789–13809. [CrossRef]
12. Melideo, D.; Baraldi, D. CFD analysis of fast filling strategies for hydrogen tanks and their effects on key-parameters. *Int. J. Hydrogen Energy* **2015**, *40*, 735–745. [CrossRef]
13. Melideo, D.; Baraldi, D.; Galassi, M.C.; Ortiz Cebolla, R.; Acosta Iborra, B.; Moretto, P. CFD model performance benchmark of fast filling simulations of hydrogen tanks with pre-cooling. *Int. J. Hydrogen Energy* **2014**, *39*, 4389–4395. [CrossRef]
14. Wang, X.; Tian, M.; Chen, X.; Xie, P.; Yang, J.; Chen, J.; Yang, W. Advances on materials design and manufacture technology of plastic liner of type IV hydrogen storage vessel. *Int. J. Hydrogen Energy* **2022**, *47*, 8382–8408. [CrossRef]
15. Woodfield, P.L.; Monde, M.; Takano, T. Heat Transfer Characteristics for Practical Hydrogen Pressure Vessels Being Filled at High Pressure. *J. Therm. Sci. Technol.* **2008**, *3*, 241–253. [CrossRef]
16. Kim, S.C.; Lee, S.H.; Yoon, K.B. Thermal characteristics during hydrogen fueling process of type IV cylinder. *Int. J. Hydrogen Energy* **2010**, *35*, 6830–6835. [CrossRef]
17. Wieme, T.; Duan, L.; Mys, N.; Cardon, L.; D'hooge, D.R. Effect of Matrix and Graphite Filler on Thermal Conductivity of Industrially Feasible Injection Molded Thermoplastic Composites. *Polymers* **2019**, *11*, 87. [CrossRef]
18. Travaš, L.; Rujnić Havstad, M.; Pilipović, A. Optimization of Thermal Conductivity and Tensile Properties of High-Density Polyethylene by Addition of Expanded Graphite and Boron Nitride. *Polymers* **2023**, *15*, 3645. [CrossRef]
19. Tavman, I.H. Thermal and mechanical properties of copper powder filled poly (ethylene) composites. *Powder Technol.* **1997**, *91*, 63–67. [CrossRef]
20. Patnaik, A.; Abdula, M.; Biswas, S.; Satapathy, A. Thermal conductivity of particulate filled polymer composites. *Mater. Sci. Indian J. (MSAIJ)* **2009**, *5*, 306–318.
21. Grundler, M.; Derieth, T.; Heinzel, A. Polymer compounds with high thermal conductivity. *AIP Conf. Proc.* **2016**, *1779*, 030015. [CrossRef]
22. Chen, H.; Ginzburg, V.V.; Yang, J.; Yang, Y.; Liu, W.; Huang, Y.; Du, L.; Chen, B. Thermal conductivity of polymer-based composites: Fundamentals and applications. *Prog. Polym. Sci.* **2016**, *59*, 41–85. [CrossRef]
23. Che, J.; Wu, K.; Lin, Y.; Wang, K.; Fu, Q. Largely improved thermal conductivity of HDPE/expanded graphite/carbon nanotubes ternary composites via filler network-network synergy. *Compos. Part A Appl. Sci. Manuf.* **2017**, *99*, 32–40. [CrossRef]
24. Babay, M.A.; Adar, M.; Touairi, S.; Chebak, A.; Mabrouki, M. Numerical Simulation and Thermal Analysis of Pressurized Hydrogen Vehicle Cylinders: Impact of Geometry and Phase Change Materials. *J. Adv. Res. Fluid Mech. Therm. Sci.* **2024**, *117*, 71–90. [CrossRef]
25. Liszka, M.; Fridlyand, A.; Jayaraman, A.; Bonnema, M.; Sishtla, C. Hydrogen Fast Fill Modeling and Optimization of Cylinders Lined With Phase Change Material. In Proceedings of the ASME International Mechanical Engineering Congress and Exposition-2020, Portland, OR, USA, 15–19 November 2020. [CrossRef]
26. Ramasamy, V.; Richardson, E.S.; Reed, P.; Hepples, W.; Wheeler, A. Investigating the use of phase-change materials for temperature control during fast filling of hydrogen cylinders. *High Temp. Mater. Process. Int. Q. High-Technol. Plasma Process.* **2018**, *22*, 73–97. [CrossRef]

27. Bard, S. Kohlenstofffaser-Epoxydharz-Verbunde mit Erhöhter Wärmeleitfähigkeit: Struktur und Eigenschaften. Ph.D. Thesis, Universität Bayreuth, Bayreuth, Germany, 2021.
28. Bard, S.; Schönl, F.; Demleitner, M.; Altstädt, V. Copper and Nickel Coating of Carbon Fiber for Thermally and Electrically Conductive Fiber Reinforced Composites. *Polymers* **2019**, *11*, 823. [CrossRef] [PubMed]
29. Liebers, N.; Ropte, S. Accelerated refueling of type IV hydrogen pressure tanks by passive means: Thermal material characterization and evaluation. In Proceedings of the EASN 2025, Madrid, Spain, 14–17 October 2025.
30. *ISO 11358-1:2022*; Plastics—Thermogravimetry (TG) of Polymers. International Organization for Standardization: Geneva, Switzerland, 2022.
31. Schürmann, H. *Konstruieren mit Faser-Kunststoff-Verbunden, 2. bearbeitete und erweiterte Auflage*; Springer: Heidelberg, Germany, 2013.
32. Mettler Toledo. *TOPEM®—The New Advanced Multi-Frequency TMDSC Technique*; Mettler Toledo: Columbus, OH, USA, 2005.
33. VDI-Gesellschaft Verfahrenstechnik und Chemieingenieurwesen. *VDI-Wärmeatlas, 11. bearbeitete und erweiterte Auflage*; Springer Vieweg: Heidelberg, Germany, 2013.
34. Bourgeois, T.; Ammouri, F.; Baraldi, D.; Moretto, P. The temperature evolution in compressed gas filling processes: A review. *Int. J. Hydrogen Energy* **2018**, *43*, 2268–2292. [CrossRef]
35. Monde, M.; Kosaka, M. Understanding of Thermal Characteristics of Fueling Hydrogen High Pressure Tanks and Governing Parameters. *SAE Int. J. Altern. Powertrains* **2013**, *2*, 61–67. [CrossRef]
36. Gebhart, T.M.; Spiller, M.; Çelik, H.; Dahlmann, R.; Hopmann, C. Experimental analyses of the spatial varying temperature development of type-IV hydrogen pressure vessels in cyclic tests considering different length to diameter ratios. *Int. J. Hydrogen Energy* **2023**, *48*, 27304–27318. [CrossRef]
37. Langtangen, H.P. Finite difference computing with PDEs: A modern software approach. In *Texts in Computational Science and Engineering*; Springer Open: Cham, Switzerland, 2017; Volume 16. [CrossRef]
38. Couteau, A.; Dimopoulos Eggenschwiler, P.; Jenny, P. Heat transfer analysis of high pressure hydrogen tank fillings. *Int. J. Hydrogen Energy* **2022**, *47*, 23060–23069. [CrossRef]
39. Monde, M.; Woodfield, P.; Takano, T.; Kosaka, M. Estimation of temperature change in practical hydrogen pressure tanks being filled at high pressures of 35 and 70 MPa. *Int. J. Hydrogen Energy* **2012**, *37*, 5723–5734. [CrossRef]
40. Lüders, C.; Ropte, S.; Schmidt, D.; Liebisch, M. Dataset on hydraulic burst pressure test of Type IV composite pressure vessel. *Data Brief* **2025**, *59*, 111333. [CrossRef]
41. Büchner, K. Pilotstudie zur Herstellung von Wasserstoff-Hochdrucktanks Mittels Thermoplastischer Radialtränkung der Faserwicklung. Master's Thesis, Otto-von-Guericke-Universität, Magdeburg, Germany, 2023.
42. Ropte, S. Verfahren und Werkzeug zur Herstellung eines Faserverbund-Hohlkörpers. DE102022103036, 9 February 2022.